Hindawi
Applied Bionics and Biomechanics
Volume 2023, Article ID 6621850, 12 pages
https://doi.org/10.1155/2023/6621850

Research Article

Kinematics Bionic Concept Structure Design and Optimization of Vehicle Crash Dummy's Knee Joint: Bionics and Biomechanics Applied in Collision Safety of Cars

Tianyi Hao,[1,2] Zhixin Liu,[3] and Hai Liu [1,2]

[1]*School of Mechanical Engineering, Hebei University of Technology, Tianjin 300130, China*
[2]*Tianjin Key Laboratory of Power Transmission and Safety Technology for New Energy Vehicles, Hebei University of Technology, Tianjin, China*
[3]*China Automotive Technology and Research Center Co, Ltd, Tianjin 300300, China*

Correspondence should be addressed to Hai Liu; liuhai@hebut.edu.cn

Received 2 December 2022; Revised 15 February 2023; Accepted 22 March 2023; Published 3 May 2023

Academic Editor: Wen-Ming Chen

The structural bionicism of the knee joint of an automobile crash dummy is an important factor affecting the accuracy of the dummy's knee displacement and knee flexion angle measurements in automobile crash tests. This study focused mainly on the optimization of the bionic structure of the knee joint of an automobile crash dummy to ensure that the dummy has a kinematic response closer to that of the knee joint of a real human. Forty sets of high-speed photographic images of the sphyrion were acquired by performing a trajectory-measurement test at the lower tibial point. Subsequently, the high-flexion motion trajectory of the knee joint was obtained by solving vector equations and by multicurve fitting. This trajectory, combined with the bionic structure design method, optimized the structure of the existing dummy's knee joint. Thereby, its motion can be altered from a fixed-axis rotation to a non-fixed-axis curve motion close to how the human tibial plateau rotates around the femoral condyle. This increases the degrees of freedom of the dummy's knee joint from two to three. The knee joint structures before and after the optimization were simulated kinematically using a multibody dynamics method. The results showed that the peak of the motion trajectory deviation of the optimized sphyrion decreased from 3.7% to 1.9%, and the average deviation decreased from 2.0% to 0.2%. This indicates that the structural optimization scheme improved the motion bionics of the crash dummy's knee joint.

1. Introduction

With the progress and development of technology and industry, car ownership is increasing continuously, and road conditions are becoming increasingly complex. The public's requirements for car safety are also increasing gradually [1]. According to statistics, the incidence of lower limb injuries is second only to that of head injuries in traffic accidents from the front. Furthermore, lower limb injuries can have long-lasting adverse physical and psychological effects on individuals [2]. As the most complex joint in the human lower limb structure, the knee joint is one of the most frequently injured joints because of its anatomical structure and its mechanical environment. Therefore, it is particularly important to optimize the knee joint structure of dummies in automobile crash tests and, thereby, obtain results of knee joint after crash, which are more consistent with the laws of human motion and response.

Structural bionic design mainly studies the design applications of the internal structural principles existing in organisms and natural substances. It is highly suitable for mechanical products. Currently, most structural bionic designs for knee joints are used in the fields of sports, health, medicine, robotics, and crash dummies.

Its application in the field of sports and health aims primarily to optimize the kinematics and dynamics model of the knee joint through the study of human gait, as well as to more accurately evaluate the posture of human movement and the stress state of the lower limbs. Bao and Willems [3] performed kinematic modeling and parameter estimation of

the human knee joint. They equated the human tibial plateau to a straight line and the femoral condyle to an involute line. Further, they verified the accuracy of their mathematical model using gait analysis tests. Shu et al. [4] used a human gait monitor to record the movement trajectory of the tibiofemoral joint in healthy males. The test results showed that the relative motion of the tibial and femoral condyles in the sagittal plane was non-fixed-axis rotation. Protopapadaki et al. [5] obtained the normal function parameters of human lower limbs by designing a gait analysis test for going up and down stairs, and the kinematic and dynamic responses during the knee flexion process were studied, which provided a research basis for theoretical joint modeling and bionic joint design.

Applications in the medical field mainly include the design of prosthetics and the improvement of artificial joints. Azocar et al. [6] improved the kinematics and dynamics bionic performance of prosthetics by extracting the kinematic trajectory of the knee and ankle joints using a combined motor-driven pulley system and four-link structure. Hood et al. [7] designed gait analysis experiments to obtain accurate lower limb swing gaps during human walking and used closed-loop adjustments to regulate the power and torque of the motor at the knee joint of the powered prosthesis, thus optimizing the maximum flexion angle of the bionic knee joint. Finally, the dynamic response of the powered prosthesis was close to that of the human standard.

In the field of robotics, bionic design is primarily used to improve the motion and force performance of robots. Binrui [8] designed a robot bionic knee joint using a four-bar linkage mechanism. This structure can provide a higher height for the foot from the ground under the same calf flexion angle, and the dynamic characteristics are closer to those of the human body. The bionic knee joint driver designed by Shenshun et al. [9] can realize motion with four degrees of freedom, and the variable curvature design of the contact interface at the upper and lower ends of the joint can effectively improve its mechanical performance.

In the field of crash dummies, there have been few studies on the bionic structure design of knee joints in recent years. A more representative study is that of Jaśkiewicz et al. [10], who applied a resistance-adjustable bearing structure to the bionic structure optimization of the Hybrid III dummy knee joint. The optimized knee kinematics and dynamic response of the dummy meet the multilevel adjustment function required for dummies of different sizes.

These indicate that the application of the bionic design method to the structural design of the knee joint can yield a kinematic response closer to that of the human lower limb. However, the existing design methods and structural models are applied mainly to the field of robot active knee joints and medical prostheses. Here, the complexity and precision of the models render these inapplicable to the structural design of the knee joint of an automobile crash dummy under impacting load conditions. Based on this problem, this study addressed the bionic performance deficiency of the knee joint fixed-axis flexion motion of existing crash dummies. It adopted a bionic design method to apply the curvature center curve of the human tibia and femoral condyle relative to the axis of rotation to the structural design of the knee joint of an automobile crash dummy. Thereby, it could be optimized to have a three-degree-of-freedom mechanism, which is closer to the real human kinematic response. This improved the accuracy of the lower limb data of the dummy in the automobile crash test. The technical route of the bionic knee joint structure optimization carried out in this study is shown in Figure 1.

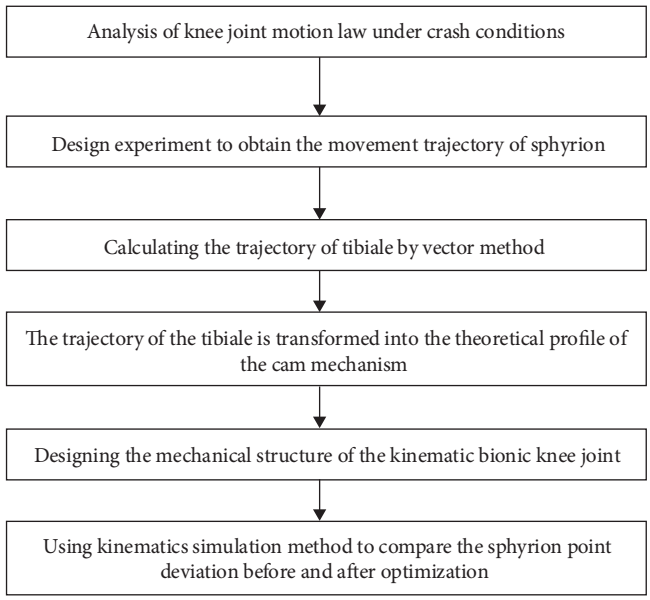

Figure 1: Design scheme of bionic knee joint.

2. Materials and Methods

2.1. Analysis of Bionic Structure of Knee Joint Movement

2.1.1. The Constitution and Movement Mechanism of Human Knee Joint. The knee joint is the most complex joint of the human body. Four bones are distributed around it: the femur, tibia, patella, and fibula. The meniscus distributed between the femur and tibia plays a role in increasing the contact area. In addition to bones, the entire knee joint is surrounded by soft tissue ligaments. Among the four major ligaments of the tibiofemoral joint, the anterior cruciate ligament (ACL) and posterior cruciate ligament (PCL) provide 85% of the restraining force for an anterior displacement of the tibia when the knee joint is flexed from 30° to 90° [11, 12].

Based on the structural composition of the knee joint, in terms of tibiofemoral kinematics, the knee joint can rotate along three axes and translate along three axes for six degrees of freedom: flexion–extension motion in the horizontal axis (motion ranging from −15° to 135°), inversion–extraction motion in the sagittal axis (motion ranging from −6° to 8°), internal and external rotation motion in the vertical axis (motion ranging from 25° to 30°), anteroposterior horizontal translation (motion ranging from 10 to 15 mm), lateral horizontal translation (motion ranging from 2 to 4 mm), and longitudinal vertical translation (motion ranging from 2 to 6 mm) [13, 14]. These motions are shown in Figures 2(a) and 2(b).

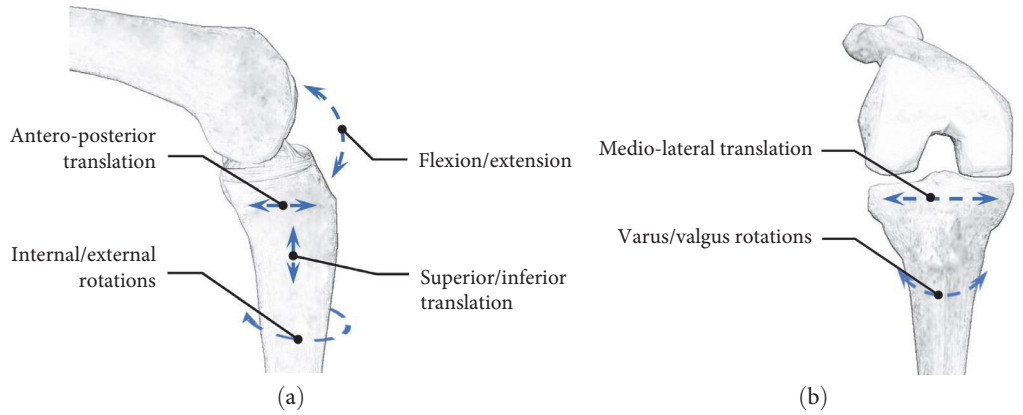

FIGURE 2: Knee joint movement: (a) left view; (b) front view.

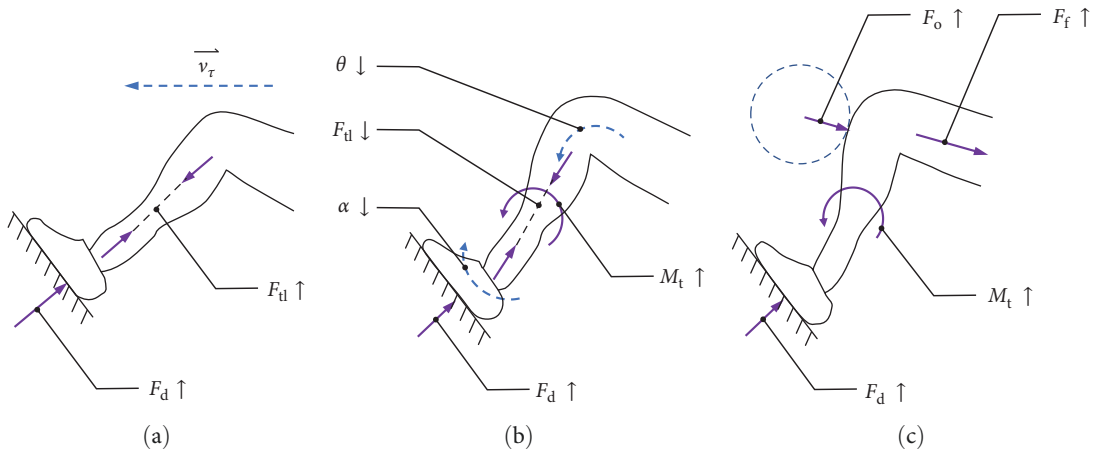

FIGURE 3: Collision process and movement form of lower limbs: (a) phase 1; (b) phase 2; (c) phase 3.

2.1.2. Kinematics of the Knee Joint Under Crash Conditions. When a vehicle is involved in a head-on accident, considering the driver as an example, the transfer process [15] of the impact force on the lower limb and form of motion includes steps 1–3 for a total of three phases (see Figure 3).

Phase 1: Inertial body movement $\overrightarrow{v_i}$ causes the reaction force of the left foot F_d to press tightly against the resting footplate. The axial force on the left lower limb tibia F_{tl} increases abruptly. This phase is shown in Figure 3(a).

Phase 2: Pedal pressure F_d increases until the left foot locks out. The ankle then begins to rotate. The ankle-to-calf pinch angle α gradually decreases. The knee pinch angle θ decreases. The tibial flexion moment M_t increases. The axial force F_{tl} decreases marginally. This phase is shown in Figure 3(b).

Phase 3: The knee patella impacts the inner trim of the wiring harness. The left ankle begins to lock longitudinally. The tibial flexion moments and thigh axial forces increase significantly. This phase is shown in Figure 3(c).

In phases 1 and 3, the kinematic characteristics of the knee joint under forced force conditions differ from the active motion state. This is because ACL plays a dominant restraining role during an autonomous movement of the human knee joint owing to the tendency of the tibia to move forward. However, when the tibial plateau sustains a violent impact, the shear load between the femur and tibia increases, and the tibia has a tendency to move backward. The PCL has the role of limiting the posterior displacement of the tibia and is subjected to tensile load. Consequently, the PCL plays a dominant restraining role and fractures when the load attains its tolerance limit [11]. In addition, with the increase in knee flexion angle, the tibial plateau generates radial displacement along the swing trajectory when swinging along the femoral condyle. Although the meniscus and articular cartilage provide a buffer, this displacement exacerbates the tibial axial force. This, in turn, reduces the stability of the tibial compression bar and increases the risk of fracture [15]. Therefore, the focus needs to be on flexion and extension movements, anterior and posterior horizontal translation, and longitudinal vertical translation of the human knee joint under head-on collision conditions.

2.1.3. Knee Joint Structure and Working Characteristics of Existing Dummy. The structure and main components of the existing Hybrid III dummy's knee include a kneecap, knee displacement slider, and knee displacement sensor

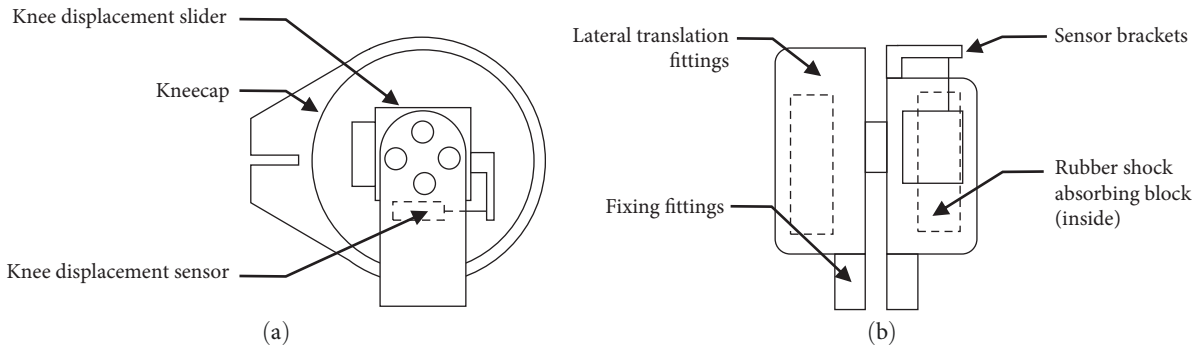

Figure 4: Schematic diagram of Hybrid III dummy knee joint structure: (a) knee joint structure; (b) knee displacement slider structure.

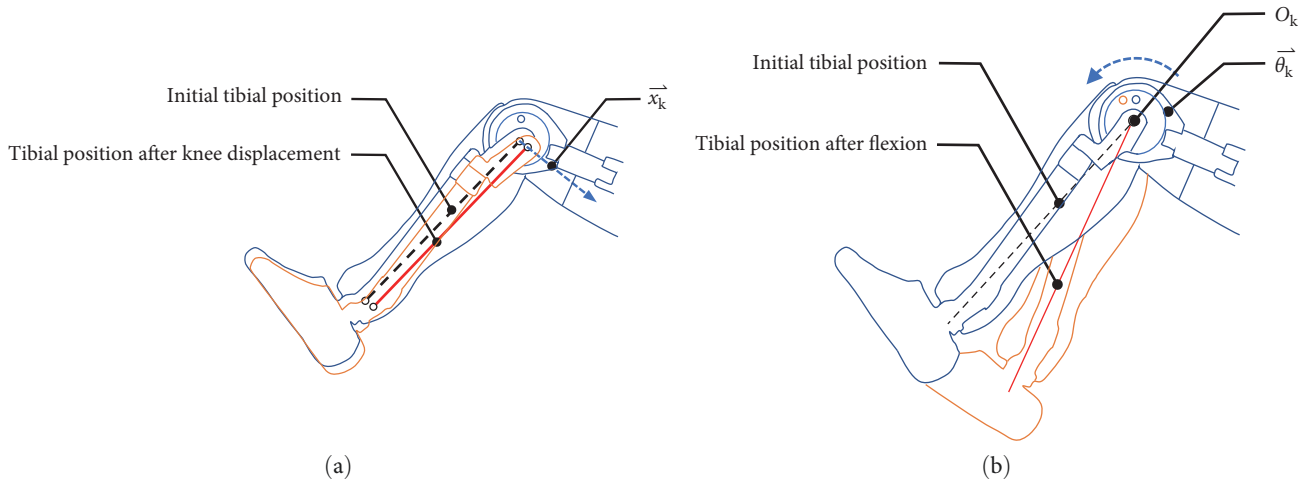

Figure 5: Schematic diagram of Hybrid III dummy knee joint movement: (a) flexion movement; (b) displacement movement.

(see Figures 4(a) and 4(b)). The knee displacement slider consists of symmetrically distributed medial fixing fittings, rubber shock absorbing blocks, lateral translation fittings, and sensor brackets [4].

The rubber shock-absorbing block is bonded to the medial fixing fitting and lateral translation fitting by vulcanization. The medial fixing fitting and the outer translation fitting can move relative to each other through slots within a range of 0–18 mm. The medial fixing fittings on both sides are connected to the center hole of the kneecap through a central bolt to form a rotating pair. The lateral translation fittings are connected to the U-shaped fork of the tibia through four bolts. This structure enables the dummy's lower leg to achieve two types of movements during the collision as follows:

(1) When the initial stage of the collision occurs, the dummy's lower leg flexion angle θ_k increases gradually owing to the impact of the vehicle floor and the dummy's inertia. The center of swing rotation is at the central bolt of the knee displacement slider O_k. The oscillation trajectory is shown schematically in Figure 5(a).

(2) The dummy's lower leg produces a backward displacement $\vec{x_k}$ perpendicular to the tibial axis when the ankle is locked, the position is fixed, and the lower side of the knee strikes the wiring harness trim plate of the steering wheel. The trajectory of this motion is shown in Figure 5(b).

The existing crash dummy's knee joint design simplifies the six degrees of freedom of the human knee joint to two degrees of freedom. This can simulate the flexion motion and anterior–posterior translation of the human lower leg relative to the thigh. However, according to the motion state of the human lower limbs during the head-on collision in Section 2.1.2, the flexion degrees of freedom along the horizontal axis affect the flexion angle of the knee, the anterior–posterior translation parallel to the sagittal plane directly affects the PCL loading conditions, and the vertical component of the relative rotation of the tibial plateau and femoral condyles affects the axial loading state of the tibia. Therefore, it is difficult to accurately simulate the motion performance of the knee joint in real collision events with the existing dummy's knee joint design scheme that simplifies the relative rolling and sliding motion between the tibia and femoral condyle to fixed-axis rotations [16]. Meanwhile, the tibial pressure and tibial bending moment measured in the crash test are affected to a certain extent owing to an insufficient consideration of the degrees of freedom of the dummy's lower limb motion state.

Table 1: The average parameters of the experimenters.

	Height (cm)	Weight (kg)	Sitting height (cm)	Tibia length (cm)	BMI
Average	176.2	78.6	89.4	35.3	22.7
Max	179.9	81.5	91.2	36.7	24.1
Min	173.8	68.6	87.3	34.4	21
Maximum relative error	1.36%	12.7%	2.34%	2.5%	7.5%

It can be observed that the design of the dummy knee structure and the selection of the equivalent model directly affect the form of motion, swing trajectory, and motion bionic performance of the lower leg. The current knee bionic structure design is categorized mainly into the following three types [13, 14]. The first type is wherein the two-dimensional motion of the medial knee joint is simplified to be "cradle-like," which is simpler, more reliable, and can describe the form of movement in partial degrees of freedom of the knee. The second type is a four-link mechanism with the cruciate ligament as the main body, which has a high degree of motion accuracy. However, its structural strength is low owing to the complexity of the structure and instability of the rod. The third type is a spiral axis structure to describe the disorderly motion of joint rotation and translation. It has a high degree of motion bionic and motion accuracy. However, it is difficult to withstand excessive impact loads because of the more precise structure.

Therefore, the main structure of the crash dummy motion bionic knee joint designed in this study would adopt the first type of equivalent model mentioned earlier. The two-dimensional motion curve is optimized through the bionic data to make it closer to the swing trajectory of a real human knee joint. The structure type is optimized to make the bionic knee joint satisfy the three degree-of-freedom characteristics: anterior–posterior horizontal translation, longitudinal vertical translation, and flexion–extension movement.

2.2. Knee Joint High-Flexion Motion Trajectory Construction

2.2.1. Trajectory Measurement Test of Lower Tibial End Point. To make the designed knee structure of a dummy both structurally realizable and human bionic, a tibial trajectory measurement test was conducted in this study to obtain the tibial plateau oscillation curve of a real human knee. To ensure data consistency, 20 healthy male participants aged 18–30 years with similar physical characteristics were selected. The average parameters are shown in Table 1.

(1) Selection and Marking of Tracking Points. It was difficult to track the swing trajectory of the tibial plateau directly by adding marker points owing to the presence of a large number of ligaments and muscles around the knee. Thus, the experiment required the selection of easy-to-measure points to obtain this trajectory curve indirectly. Based on anthropometry, the tibial length is the tibial height minus the sphyrion height at the 90° knee flexion. The axial compression rate of the tibia under gravity is negligible, and the tibia can be regarded as a rigid two-force bar. Therefore, the swing curve of the tibial plateau around the femoral condyle can be calculated by tracing the swing trajectory of the sphyrion.

To obtain the marker points accurately, the participant should sit flat on the measuring table. The table height should be increased to obtain the appropriate position such that the thigh is perpendicular to the lower legs. The instep is placed flat on the footbed box. Two laser gradienters are placed directly in front of and at an angle of 45° to the right of the participant, respectively. Thereby, the intersection of the horizontal laser line and plumb laser line is located at the tibiale and sphyrion. Here, the tibiale is in the depression of the patellar ligament below the patella of the bent knees. The intersection point of the front horizontal laser and the side plumb laser is defined as the projection point of the tibiale on the inner lower leg. The point on the plumb laser line 10 cm above the sphyrion is defined as the test auxiliary point. The special marker for high-speed photography should be pasted at the sphyrion, the auxiliary point, and the projection point of the tibiale. This is shown in Figures 6(a) and 6(b). Here, ① and ② are the trajectories of the sphyrion point and the auxiliary point measured in the test, respectively; ③ is the length of the tibia measured at the instant when the subject's lower leg is perpendicular to the ground; and ④ is the proposed motion trajectory of the tibiale point obtained by calculating the previous data.

(2) Acquisition of the Trajectory of Tracking Points. The test was performed using high-speed photography. The camera lens was at a distance of 5 m from the participant's projection point of the marked tibiale point. The three markers on the left side of the tibial swing test platform constituted the image reference. The adjacent interval of the marker points was 20 cm. The subject needs to bend his lower legs rapidly from the horizontal position to the limit to obtain the complete motion process of the knee joint with high flexion. The relative coordinates of the sphyrion point [7, 9, 17], the auxiliary point, and the projection point of the tibiale in the image reference coordinate system were captured continuously by high-speed photography. The swing trajectory curves of the three points can be obtained using the Falcon high-speed motion image analysis software program. Each participant was required to perform three tests. The test process is shown in Figure 7. Forty sets of valid trajectory curves were obtained by excluding the curves with large fluctuations caused by irregularities in the test movements.

2.2.2. Knee Flexion Trajectory Acquisition.

(1) Trajectory Conversion from the Sphyrion Point. According to the test results in Section 2.1, each set of test curves contains the trajectories of the sphyrion point A, the auxiliary point B, and the projection point C of the tibiale in

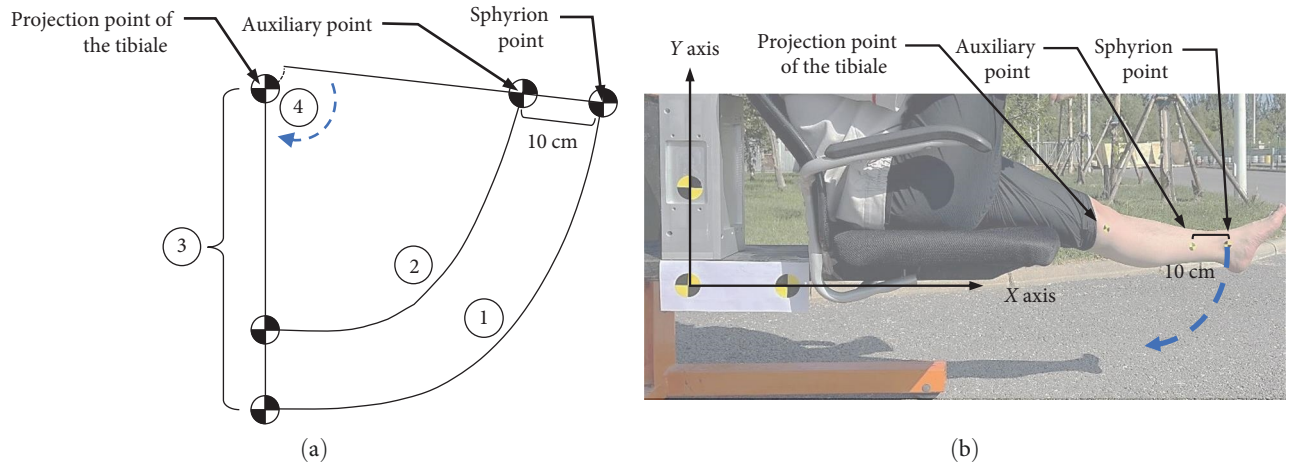

Figure 6: Marker positioning method: (a) experimental schematic; (b) experimental scene.

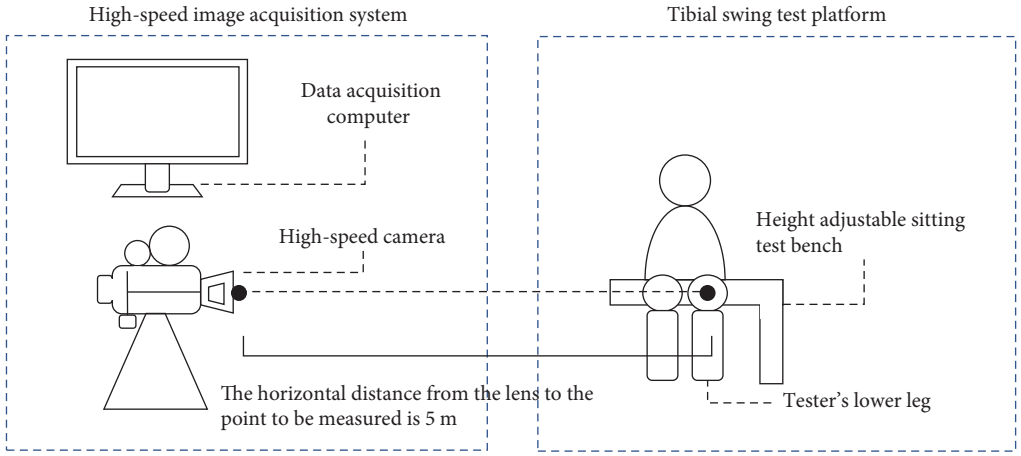

Figure 7: High-speed photography scene construction.

the swing cycle of the lower legs of a participant. Comparisons should be aligned with the same characteristic point of the trajectory to ensure that the trajectories of the sphyrion points are comparable and that their shapes are invariable across participants. According to the definition of point C, significance exists if and only if the participant's femur is perpendicular to the tibia, i.e., $|\overrightarrow{A_1C_1}|$ is the length of the participant's lower leg. In the remaining time, the flexed knee results in a large amount of displacement of the ligaments and skin around the kneecap. Consequently, point C is not located on the extension line of $\overrightarrow{AB}$. Therefore, the coordinates of point C at the instant when the participant's femur was perpendicular to the tibia were selected as the origin reference to establish a new coordinate system with the coordinate origin $O(x_O, y_O)$ and the direction of the coordinate system parallel to the image reference system (see Figure 8).

After converting the 40 sets of valid trajectory curves of sphyrion point into theoretical tibiale point curves, the portion of the curve outside the 0°–135° swing range was cropped. A multicurve fitting was performed with the fitting process shown in Figure 9. In the figure, under the new coordinate system, C' point is defined as the theoretical tibiale point. Furthermore, C' coincides with C if and only if the participant's femur is perpendicular to the tibia. The coordinates of the sphyrion point at any instant during the test are set as $A_1(x_{A1}, y_{A1})$. The coordinates of the auxiliary point at that instant are set as $B_1(x_{B1}, y_{B1})$. Thus, the coordinates of the theoretical tibiale point C' at any instant are shown in Equation (1).

$$\overrightarrow{OC_1'} = \overrightarrow{OA_1} + \frac{\overrightarrow{A_1B_1}}{|A_1B_1|} \cdot |\overrightarrow{AC_1'}|. \tag{1}$$

The following results were obtained using a five-fold polynomial fitting:

$$y = 3.153x + 122.040x^2 + 1896.149x^3 - 295.976x^4 - 221328.090x^5 + 0.443 \tag{2}$$

The theoretical tibiale point was always in the same horizontal plane as the subject's true tibiale point. Consequently,

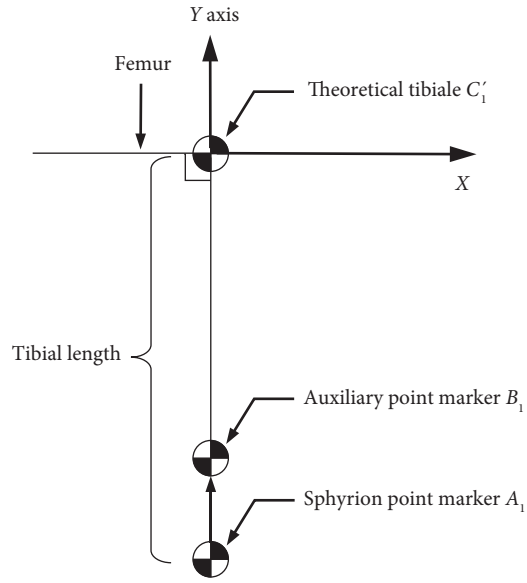

Figure 8: Schematic diagram of multitrajectory curve coordinate system transformation.

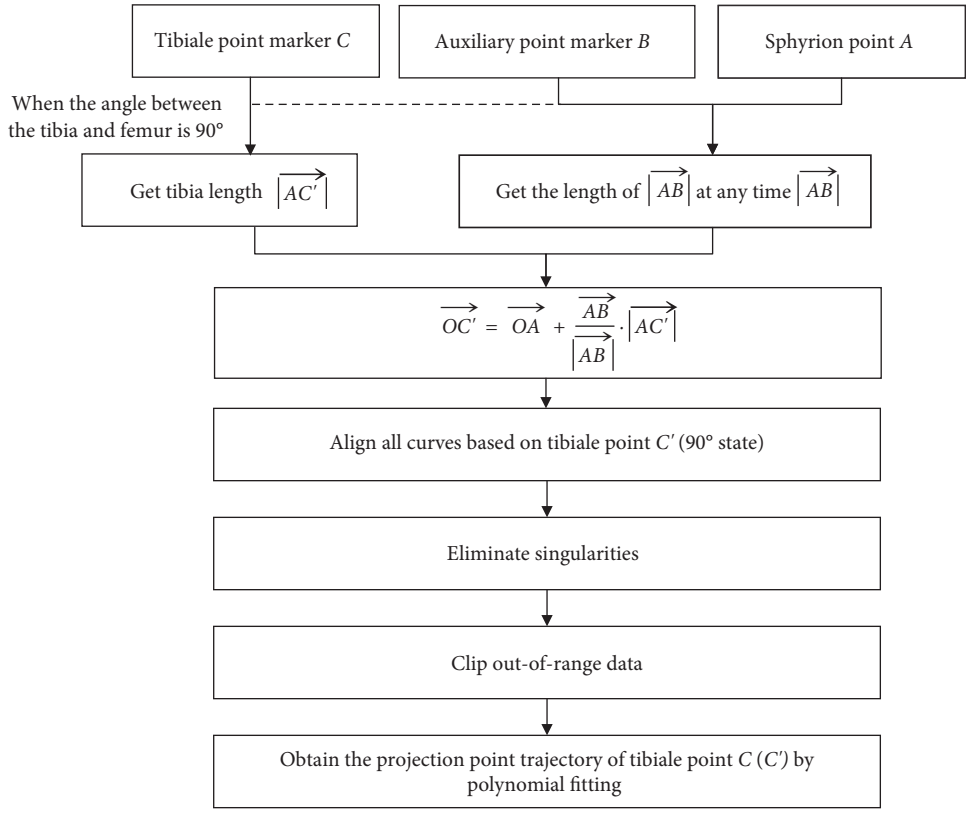

Figure 9: Curve fitting flowchart.

the resulting curve was the high-flexion trajectory of the knee (see Figure 10). The right end point of the curve is the starting point of the swing of the tibiale point in the sitting position, which corresponds to the average coordinates of the tibiale point at the instant when the lower leg is parallel to the ground in the test data. The left endpoint is the ending point. It corresponds to the average coordinates of the tibiale point at the instant when the lower leg is flexed to the limit position in the test data.

2.3. Optimal Design of Bionic Knee Joint Structure

2.3.1. Tibial Swing Bionic Curve Design. Considering the mechanism motion law, by adding the cam mechanism [18] with the bionic curve of the tibial swing as the actual

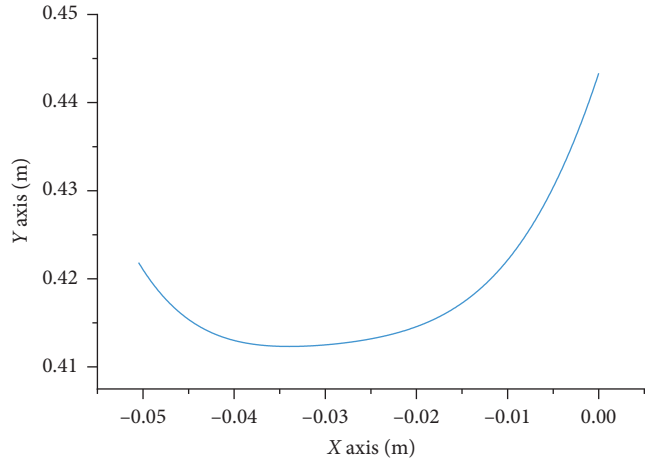

Figure 10: Fitting curve of tibial upper point motion trajectory.

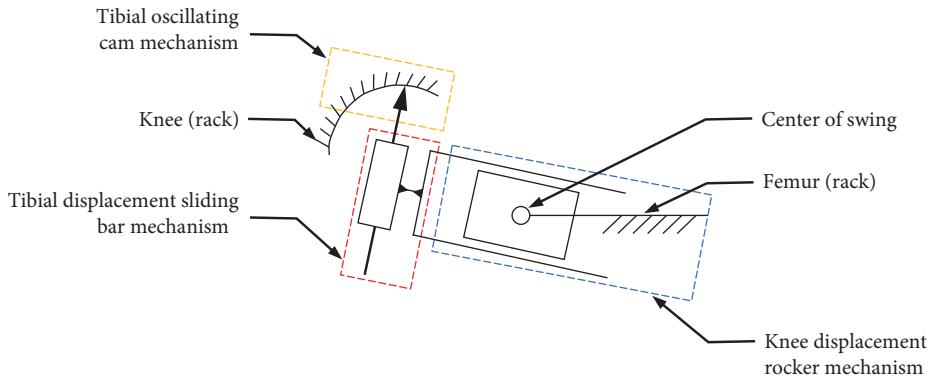

Figure 11: Motion diagram of dummy knee joint mechanism.

contour and the sliding bar mechanism and rocker mechanism for increasing the degrees of freedom for the tibial displacement, the new structure can both satisfy the knee displacement measurement of the existing dummy and achieve the knee flexion bionic motion. A sketch of the mechanism motion is shown in Figure 11.

The form of motion of the active end of the cam mechanism of tibial swing is fixed-axis rotation. The formation of its theoretical contour requires the determination of the radial offset within the working range of the cam. The high-flexion trajectory of the knee joint obtained in Section 2.2 was transformed into the polar coordinate form, as shown in Equation (3).

$$r\sin\theta = 3.153r\cos\theta + 122.040r^2\cos^2\theta + 1896.149r^3\cos^3\theta - 295.976r^4\cos^4\theta - 221328.090r^5\cos^5\theta + 0.443, \quad (3)$$

where θ is the polar angle of the knee flexion trajectory in the polar coordinate system and r is the instantaneous radius of rotation at different θ ($\theta \in (0, 3/4\pi)$).

Considering $r_b = 38$ mm as the radius of the base circle of the cam mechanism, the theoretical contour of the cam mechanism in the range of 0°–135° was obtained, as shown in Figure 12.

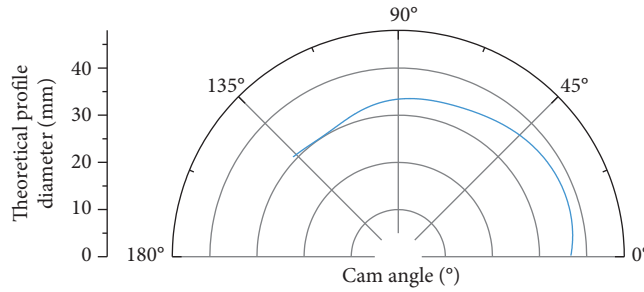

Figure 12: Cam mechanism theoretical profile.

A schematic diagram of the movement trajectory of the dummy's knee joint applying this cam mechanism is shown in Figure 13. Here, r_0 and r_θ are the instantaneous radii of rotation of the tibia point around the center axis of the kneecap for the existing and structurally optimized dummies, respectively.

2.3.2. Mechanical Structure Design. The bionic knee structure of a crash-test dummy is mainly composed of two parts: knee displacement assembly and tibia assembly. Their 3D-rendered

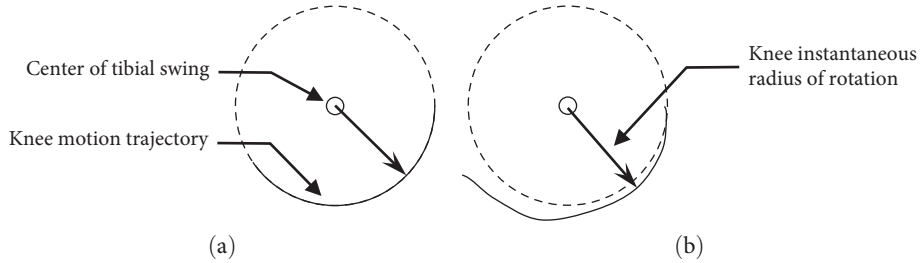

Figure 13: Cam mechanism theoretical profile: (a) existing dummy knee joint motion form; (b) knee joint motion form after structural optimization.

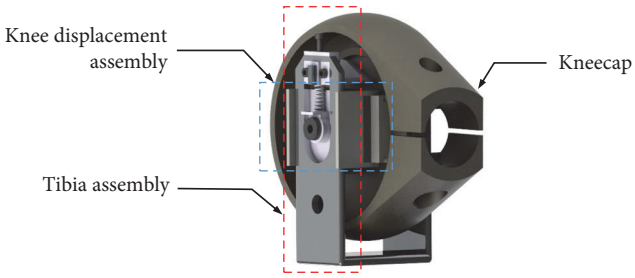

Figure 14: Overall structure design of bionic knee joint.

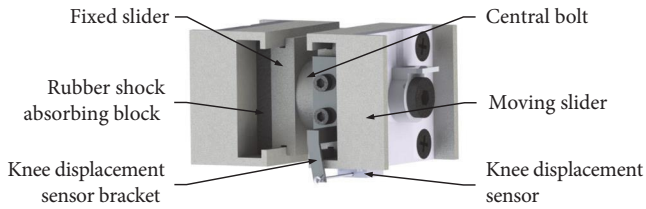

Figure 15: Knee displacement assembly structure.

view is shown in Figure 14. The kneecap is the carrier of the entire joint. The guide tracks are arranged symmetrically in the depressions on both sides to simulate the knee flexion motion trajectory. In order to ensure the replaceability of the new structure, the overall size of the kneecap is basically the same as that of the current dummy. And it is consistent with the positioning of the mounting hole of the femoral force sensor and the threaded hole. The knee displacement assembly is assembled symmetrically on both sides of the kneecap, with a fixed end and mobile end on each side. This is to measure the relative displacement of the two, and thereby, determine the knee displacement of the knee joint along the horizontal axis. The tibial assembly is embedded in the slots of the mobile ends on both sides of the knee displacement assembly. The tops of the two ends form mobile pairs by means of guide arms and kneecap guide tracks. These achieve the bionic flexion motion of the knee joint of the dummy. The knee flexion angle can be calculated by measuring the displacement of the axial motion of the tibial assembly.

(1) Design of Knee Displacement Assembly. The knee displacement assembly consists mainly of the inner and outer knee displacement slider assemblies and the knee displacement sensor, as shown in Figure 15. The outer knee displacement slider assembly includes the outer fixed slider, outer moving slider, outer rubber shock absorbing block, knee displacement sensor bracket, and knee displacement sensor.

The stabilizing arm of the outer moving slider and the slide rail of the outer fixed slider form a moving pair. This enables the two to produce relative displacement along the axis of the slide rail direction. However, these cannot undergo relative motion along the normal direction. Consequently, the two adopt a clearance fit. A rubber shock-absorbing block is placed in the gap between the fixed slider of the mobile slider. The three are bonded by vulcanization to form a knee displacement sliding system. The central fastening bolt (whose total length does not exceed the sum of the thicknesses of the inner and outer fixed sliders and the central surface of the kneecap) is used to assemble the two components on both sides of the kneecap through concentric through-holes in the center of the knee displacement slider assembly and the end surface of the knee. After appropriate preloading, the bilateral knee displacement slider assembly can be rotated about the axis of the through-holes. Meanwhile, the length of the central fastening bolt ensures that it does not interfere with the translation of the bilateral knee displacement sliders.

The knee displacement sensor bracket is bolted to the front end face of the outer fixed slider. The line displacement sensor is mounted to the lower end face of the outer moving slider. The sensor lasso end is fixed to the top of the bracket sensor. In order to ensure the versatility of the existing sensors, the sensor installation aperture and relative position provided by the structure are consistent with the current dummy. When the two sliders are displaced relative to each other along the slide axis direction, this line displacement sensor can record the displacement data in the time domain. It is used to simulate and calculate the sliding of the tibia and femoral condyles along the sagittal plane of the passenger in the vehicle.

(2) Design of Tibial Assembly. The tibial assembly consists of a kneecap and tibial connector, as shown in Figure 16. It consists of a U-shaped fork, bilateral guide arms, bilateral preload adjustment bolts, bilateral slider covers, and PCL simulator springs.

In order to keep the initial position of the tibiale point in the new structure consistent with that of the current dummy, the distance from the initial rotation center of the U-shaped fork to the bottom surface is designed to be equal to the

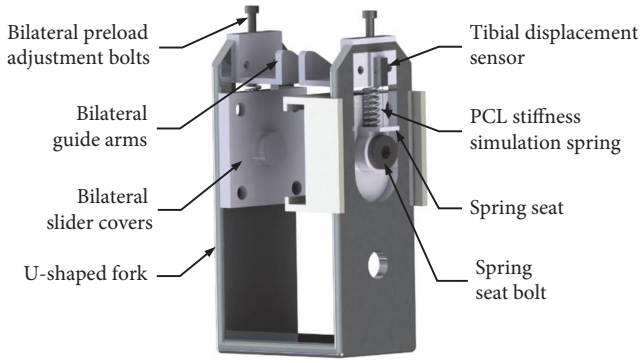

Figure 16: Tibial displacement assembly structure.

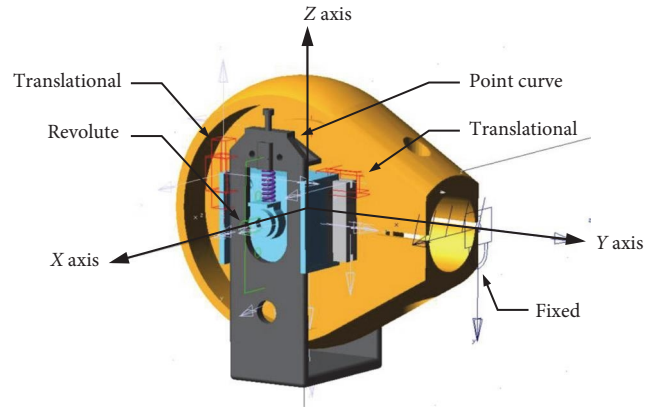

Figure 17: Kinematics simulation constraint establishment.

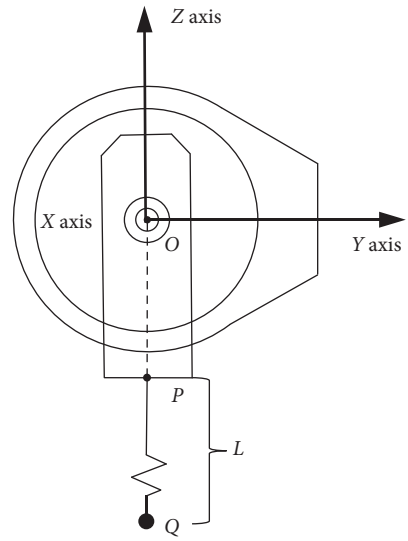

Figure 18: Kinematics simulation tracking points.

length of the current dummy. The bilateral slider cover plates are bolted to the outer surface of the mobile slider in the knee displacement assembly. This plane is the working surface of the U-shaped fork. It forms a "C-shaped" mobile slot of the tibial joint connector in conjunction with the front and rear shoulders of the mobile slider. Thereby, the U-shaped fork can move in the slots in the direction of restraint while swinging with the knee displacement assembly. The guiding arm is a G-shaped metal block bent toward the central symmetrical surface of the kneecap. It is bolted to the spring cover and U-shaped fork on the outside. The curved top surface on the inside is tangential to the guiding track arranged symmetrically in the depressions on both sides of the kneecap so that the U-shaped fork is permitted to oscillate while the top surface of the guiding arm presses against the guiding track to form a bionic knee curve sliding. The lower end of the PCL simulating spring is mounted in the spring seat. The upper end extends into the cylindrical surface formed by the spring cover and U-shaped fork. The top is in contact with the preload adjusting bolt. The guiding groove of the slider cover ensures that the spring undergoes stretching motion only in the axial direction.

3. Results and Discussion

3.1. Kinematic Analysis

3.1.1. Simulation Model Building. A kinematic model of the dummy's knee joint with the geometric parameters as the parameters were established to verify whether the motion law of the structurally optimized dummy's knee joint satisfies the design requirements. The change law of the corresponding coordinates of the sphyrion point with time was studied using the multibody dynamics method. A spatial coordinate system was established with the outer side of the central hole of the knee bone of the dummy as the positive X-axis direction, the outer side of the femoral joint hole as the positive Y-axis direction, and the upper side of the knee bone as the positive z-axis direction.

The flexion motion of the knee joint is the main motion state. Only relative rotation occurs between the knee displacement assembly and the kneecap. It can be considered a rotation pair with one degree of freedom. Only relative sliding occurs between the knee displacement fixed slider and the translation slider. These can be considered a sliding pair with one degree of freedom. Both relative sliding and rolling occur between the guiding arm and kneecap. These can be considered a cylindrical higher pair with four degrees of freedom. Only relative sliding occurs between the tibial U-shaped fork and the knee-displacement assembly. These can be regarded as a sliding pair with one degree of freedom. When the tibia assembly is in the swing state, the kneecap is the central component of the mechanism. It is connected to the ground as the frame. The coordinate system and constraint settings are shown in Figure 17.

3.1.2. Simulation Results. The projection point P of the origin O of the coordinate system in the 90° flexion state of the dummy's knee at the lower end face of the U-shaped clamp is considered the starting point. The point Q is set with the offset distance L along $\overrightarrow{OP}$ direction as the tracking point of the kinematic. This is shown in Figure 18. Here, L is the average tibial length of the participants in Section 2.1.

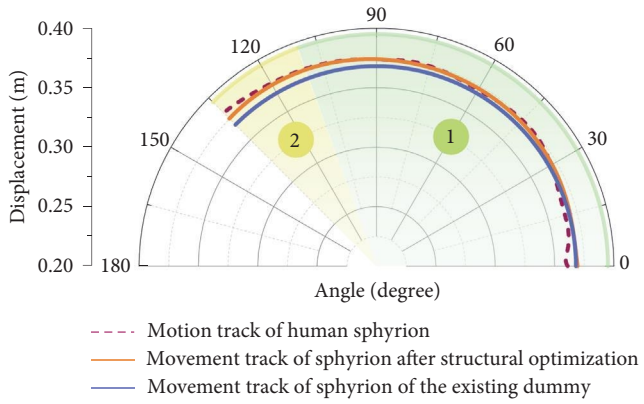

Figure 19: Comparison of polar coordinates of the trajectory of the sphyrion point before and after the optimized structure.

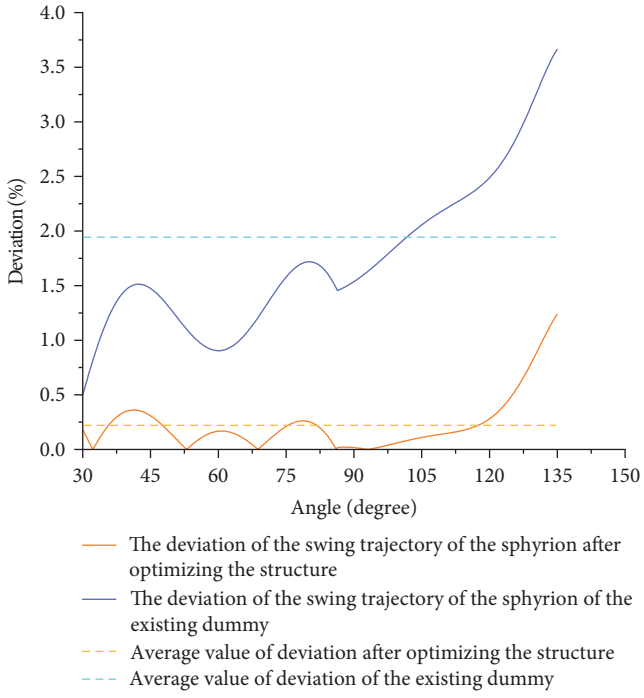

Figure 20: Comparison of trajectory deviation of the sphyrion point after optimized structure.

Considering that the initial angle of the human knee in the vehicle driving posture model is generally larger than 30° [19], the range of the input parameter (the polar angle of the knee flexion trajectory) is selected from 30° to 135°. Among these, region 1 is the active motion range of the low flexion of human knee joint, $\theta \in (30°,110°)$, and region 2 is the passive motion range of the high flexion of human knee, $\theta \in (110°, 135°)$. The comparison of the swing trajectory of the sphyrion point before and after optimization is shown in Figure 19.

The deviation of the dummy's tibial swing trajectory relative to the human lower leg swing trajectory was calculated separately for the existing dummy and the dummy with optimized structure at an equal polar angle. The results are shown in Figure 20. The peak deviation of the trajectory of the existing structure is 3.7%, with an average deviation of 2.0%. The peak deviation of the trajectory after the structure is optimized is 1.9%, with an average deviation of 0.2%.

Admittedly, this study is limited by the fact that the sample processing with a long period and the calibration test equipment do not meet the needs. This paper only verifies the effectiveness of the model for improving the bionic performance of the crash dummy's knee joint through kinematics simulation. At present, we are conducting 3D-printing verification of the model and will carry out sample trial production and relevant calibration experiments soon. The model was further verified to improve the dynamic performance of the dummy's knee joint, and the repeatability and reproducibility of the measured results of the component were tested.

4. Conclusions

(1) In this study, the structural differences between existing automobile crash dummy's knee joints and real human knee joints were identified and analyzed. Combining this with the motion forms of the knee joints under crash conditions, the study applied bionic structural design methods, the cam mechanism, the sliding bar mechanism, and the rocker block mechanism to optimize the structure of a crash dummy's knee joint. Thereby, the two degrees of freedom model of the existing dummy's knee joint was optimized to three degrees of freedom, and the motion bionic structure was improved.

(2) By designing a measurement test of the swing trajectory of the lower tibial point in the human sitting posture, 40 sets of motion trajectories of the sphyrion point and the auxiliary point swinging from the horizontal to the 135° high-flexion position were recorded using high-speed photography and supporting facilities. The swing curve of the knee was obtained by solving vector equations and using a multicurve fitting algorithm. The curve was used for the theoretical contour design of the cam mechanism of the bionic knee.

(3) The kinematic simulation analysis of the knee joint structure of the dummy before and after optimization using the multibody dynamics method revealed the following: by optimizing the fixed-axis rotation of the existing dummy's knee joint into a non-fixed-axis curve motion with bionic performance, the peak deviation of the motion trajectory decreased from 3.7% to 1.9%, and the average deviation decreased from 2.0% to 0.2%. Furthermore, a significant decrease in the degree of deviation of the high-flexion phase could be observed. The improved design of the knee joint structure enhances the bionic characteristic of the knee joint motion of the crash dummy.

Data Availability

The data used to support the findings of this study are available from the corresponding author upon request.

Conflicts of Interest

The authors declare that they have no conflicts of interest.

References

[1] L. Gaylor, M. Junge, and S. Abanteriba, "Effectiveness of vehicle passive safety systems in lateral fixed-object collisions," *International Journal of Vehicle Safety*, vol. 10, no. 3-4, pp. 195–211, 2019.

[2] G. Marasini, F. Caleffi, L. M. Machado, and B. M. Pereira, "Psychological consequences of motor vehicle accidents: a systematic review," *Transportation Research Part F: Traffic Psychology and Behaviour*, vol. 89, pp. 249–264, 2022.

[3] H. Bao and P. Y. Willems, "On the kinematic modeling and the parameter estimation of the human knee joint," *Journal of Biomechanical Engineering*, vol. 121, no. 4, pp. 406–413, 1999.

[4] L. Shu, K. Yamamoto, R. Yoshizaki, J. Yao, T. Sato, and N. Sugita, "Multiscale finite element musculoskeletal model for intact knee dynamics," *Computers in Biology and Medicine*, vol. 141, Article ID 105023, 2022.

[5] A. Protopapadaki, W. I. Drechsler, M. C. Cramp, F. J. Coutts, and O. M. Scott, "Hip, knee, ankle kinematics and kinetics during stair ascent and descent in healthy young individuals," *Clinical Biomechanics*, vol. 22, no. 2, pp. 203–210, 2007.

[6] A. F. Azocar, L. M. Mooney, J.-F. Duval, A. M. Simon, L. J. Hargrove, and E. J. Rouse, "Design and clinical implementation of an open-source bionic leg," *Nature Biomedical Engineering*, vol. 4, pp. 941–953, 2020.

[7] S. Hood, S. Creveling, L. Gabert, M. Tran, and T. Lenzi, "Powered knee and ankle prostheses enable natural ambulation on level ground and stairs for individuals with bilateral above-knee amputation: a case study," *Scientific Reports*, vol. 12, Article ID 15465, 2022.

[8] W. Bin-rui, "Study on four-bar linkage bionic knee joint of bipedal robots," *Journal of Machine Design*, 2006.

[9] Y. Shenshun, Q. Xiansheng, and Z. Ren, "Bio-mimetic joint actuator imitating the function of human knee," *Mechanical Science and Technology for Aerospace Engineering*, no. 11, pp. 1501–1506, 2007.

[10] M. Jaśkiewicz, D. Frej, and B. Šarkan, "Construction of the knee joint of the dummy designed for crash tests," *Transportation Research Procedia*, vol. 44, pp. 121–128, 2020.

[11] G. Li, L. E. DeFrate, H. Sun, and T. J. Gill, "In vivo elongation of the anterior cruciate ligament and posterior cruciate ligament during knee flexion," *The American Journal of Sports Medicine*, vol. 32, no. 6, pp. 1415–1420, 2004.

[12] K. A. Schafer, S. Tucker, T. Griffith et al., "Distribution of force in the medial collateral ligament complex during simulated clinical tests of knee stability," *The American Journal of Sports Medicine*, vol. 44, no. 5, pp. 1203–1208, 2016.

[13] C. Huber, Q. Zhang, W. R. Taylor, A. A. Amis, C. Smith, and S. H. H. Nasab, "Properties and function of the medial patellofemoral ligament: a systematic review," *The American Journal of Sports Medicine*, vol. 48, no. 3, pp. 754–766, 2020.

[14] B. Innocenti, "Biomechanics of the knee joint," in *Human Orthopaedic Biomechanics*, pp. 239–263, Academic Press, 2022.

[15] A. Leledakis, J. Östh, J. Davidsson, and L. Jakobsson, "The influence of car passengers' sitting postures in intersection crashes," *Accident Analysis & Prevention*, vol. 157, Article ID 106170, 2021.

[16] C. Masson, C. Cavallero, and C. Brunet, "Impact response of Hybrid III dummy and cadaver knee-femur-pelvis complex," *International Journal of Crashworthiness*, vol. 8, no. 6, pp. 629–637, 2003.

[17] A. D. Georgoulis, A. Papadonikolakis, C. D. Papageorgiou, A. Mitsou, and N. Stergiou, "Three-dimensional tibiofemoral kinematics of the anterior cruciate ligament-deficient and reconstructed knee during walking," *The American Journal of Sports Medicine*, vol. 31, no. 1, pp. 75–79, 2003.

[18] L. Gao, C.-J. Ma, N. Zhou, and L.-J. Zhao, "Optimization design method of upper limb exoskeleton cam mechanism's motion trajectory model," *Computers & Industrial Engineering*, vol. 171, Article ID 108427, 2022.

[19] Song Changhong, Bi Xian, and Gou Junjie, "Seating reference point analysis based on ergonomics comfort, [A]," in *Proceedings of the 2014 SAE-China Congress Seclected Papers [C]*, pp. 1464–1468, 2014.